# Hemodynamic Risk Assessment in Stenotic Arteries

Computational Fluid Dynamics (CFD) Analysis of Arterial Stenosis

SBEG201 – Biotransport

## 1 Introduction

The common femoral artery (CFA) -shown in Figure 1 - was selected due to its clinical importance in peripheral arterial disease (PAD), a condition caused by atherosclerotic plaque accumulation in lower-limb arteries. Stenosis in the CFA can significantly reduce blood supply to the extremities, leading to intermittent claudication and, in severe cases, critical limb ischemia [1].

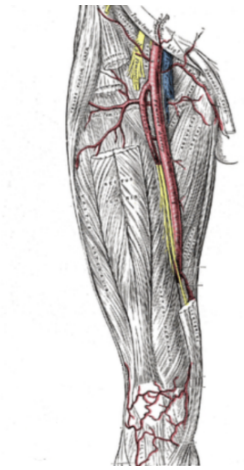

Figure 1: Common Femoral Artery

## 2 Input Justification

From a hemodynamic perspective, the CFA is a large conduit artery where flow acceleration, viscous losses, and post-stenotic flow separation are pronounced under diseased conditions, making it well suited for CFD-based pressure drop and wall shear stress (WSS) analysis. The flow was assumed to be steady and non-pulsatile.

Literature reports indicate that the healthy CFA has an internal diameter ranging from 6–10 mm [2]. In this study, a representative diameter of 6.9 mm and a length of 43.3 mm were used [3]. The resting volumetric flow rate of the CFA is 344 ml/min [4], corresponding to an inlet velocity of 0.153 m/s.

Blood exhibits non-Newtonian, shear-thinning behavior. The Carreau–Yasuda model was employed to capture this behavior. The apparent viscosity is defined as:

$$\eta(\dot{\gamma}) = \eta_\infty + (\eta_0 - \eta_\infty)\left[1 + (\lambda\dot{\gamma})^a\right]^{(n-1)/a} \qquad (1)$$

where $\eta_0 = 0.056$ Pa s, $\eta_\infty = 0.00345$ Pa s, $\lambda = 1.902$ s, $a = 1.25$, and $n = 0.22$.

## 3 Geometry Creation and Meshing

The arterial geometry was constructed using an axisymmetric modeling approach to reduce computational cost while preserving the essential three-dimensional flow physics. A two-dimensional planar profile representing half of the artery cross-section was first created and subsequently revolved about the symmetry axis to generate the three-dimensional fluid domain.

To enable local mesh control and accurate boundary condition assignment, the model was divided into three longitudinal regions: inlet, stenosis, and outlet. All boundary surfaces were defined as named selections, including the inlet face (velocity inlet), outlet face (pressure outlet), symmetry plane (axisymmetric condition), and arterial walls (no-slip condition). The stenotic and healthy wall regions were treated separately to allow targeted mesh refinement within the diseased segment.

Stenosis severity was defined based on percentage area reduction according to:

$$\%AreaReduction = (1 - \frac{A_{throat}}{A_{inlet}}) \times 100\% \qquad (2)$$

Three models were generated: a healthy artery (0%), a moderate stenosis (50%), and a severe stenosis (75%), shown in Figure 3. The stenosis geometry was implemented using a smooth cosine-shaped profile to ensure biological realism and avoid artificial flow disturbances caused by sharp geometric transitions.

Mesh generation was performed using the MultiZone method combined with a sweepable body approach to maximize the use of hexahedral elements. Hexahedral meshes were selected due to their superior numerical accuracy and improved convergence behavior when resolving velocity and shear gradients. Global element sizing was set to 0.3mm, with additional body sizing of 0.2mm to improve overall mesh uniformity. Local face sizing of $5 \times 10^{-2}$ mm was applied selectively at the stenosis wall to resolve the high velocity and pressure gradients present at the throat and in the post-stenotic region.

Inflation layers were applied along the arterial walls to ensure accurate computation of wall shear stress (WSS). A first-layer thickness of $5 \times 10^{-3}$ mm was used with eight inflation layers and a growth rate of 1.2. This configuration ensured that the near-wall mesh adequately resolved the viscous sublayer, allowing precise capture of velocity gradients critical for reliable WSS estimation.

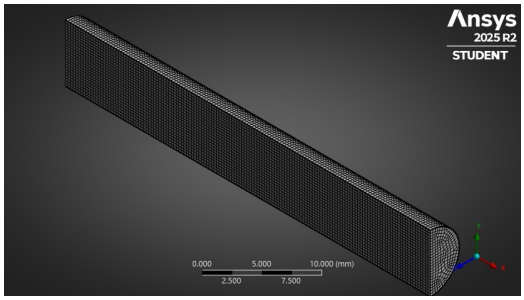


Figure 2: Healthy artery mesh

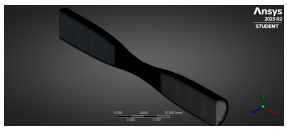

(a) Moderate mesh

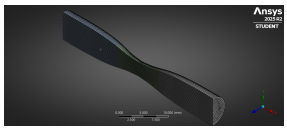

(b) Severe mesh

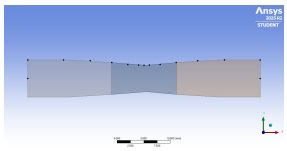

(c) Moderate geometry

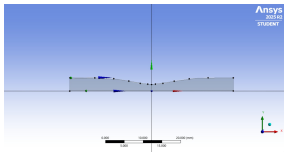

(d) Severe geometry

Figure 3: Stenotic arteries meshes and geometry

# 4 Simulation Methodology

To accurately simulate the physiological behavior of blood flow within a severely stenotic artery, the flow regime was defined as laminar for Model 4. This choice was justified not only by the calculated Reynolds number at the stenosis throat, which remained below the critical transition threshold, but also by the necessity to preserve the non-Newtonian characteristics of blood. Turbulence models in ANSYS Fluent introduce an effective eddy viscosity that dominates the momentum equations, thereby masking the shear-rate-dependent viscosity variations inherent to non-Newtonian fluids. Since the primary objective of this study was to investigate shear-thinning effects, the laminar flow assumption was essential to ensure that the Carreau viscosity model directly governed the fluid behavior.

Boundary conditions were applied to the 75% stenotic arterial geometry to replicate resting hemodynamic conditions in a large peripheral artery. The inlet was defined as a velocity inlet with a uniform magnitude of 0.153 m/s. The outlet was defined as a pressure outlet with a gauge pressure of 0 Pa. A standard no-slip boundary condition was applied to all arterial walls, enforcing zero velocity at the fluid–wall interface.

The simulations were performed using the pressure-based solver in ANSYS Fluent with double-precision arithmetic enabled to accurately resolve steep velocity and wall shear stress gradients associated with severe stenosis. Standard initialization, computed from the inlet boundary condition, was employed to establish a stable initial velocity field. The solution was then iteratively advanced until convergence was achieved, as confirmed by residual reduction and stabilization of monitored hemodynamic quantities.

# 5 Geometric Analysis

The pressure drops ) was evaluated across the length of the artery for three different stenosis severities. The results obtained from the CFD simulation are summarized in Table 1

Table 1: Pressure drop for varying stenosis severity

| Model | Classification | Stenosis (%) | $\Delta P$ (Pa) |
|---|---|---|---|
| 1 | Healthy | 0 | 15.203 |
| 2 | Moderate | 50 | 27.985 |
| 3 | Severe | 75 | 84.583 |

Discussion of Non-Linearity: The plotted curve demonstrates a distinct non-linear relationship between stenosis severity and pressure drop, consistent with the theoretical Young's Curve shown in Figure 4.

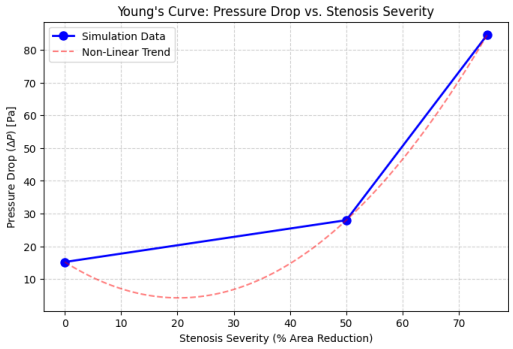


Figure 4: Young's Curve: Pressure drop vs stenosis severity

In the first part (0% to 50%) The curve is relatively flat. The pressure drops increases only marginally.

In the second part (50% to 75%+) A tipping point is reached. As the lumen area reduces further, the pressure drop spikes dramatically to 85 Pa. This rapid escalation confirms that hemodynamic resistance is inversely proportional to the fourth power of the radius (according to Poiseuille's Law for laminar flow, meaning even small geometric changes in a severe stenosis result in massive pressure losses.

The non-linear hemodynamic behaviour of arterial stenosis explains the often "silent" progression of cardiovascular disease. Patients with up to 50% blockage typically remain asymptomatic because the pressure drop is negligible, and standard check-ups may fail to detect significant impairment. However, once the stenosis exceeds a critical threshold of approximately 60-70%, the physics of flow resistance changes drastically; even minor additional plaque growth triggers an exponential spike in pressure loss. This geometric sensitivity means a patient can rapidly transition from a stable condition to critical ischemia without a gradual worsening of symptoms, as hemodynamic stability crashes suddenly rather than deteriorating linearly.

# 6 Rheological Comparison

Visual observation shows that the non-Newtonian model -shown in Figure 5- exhibits a distinctively longer post-stenotic recirculation zone compared to the Newtonian approximation. This discrepancy is driven by the shear-thinning behaviour of blood; as flow accelerates through the high-shear region of the stenosis throat, the local viscosity drops significantly, reducing viscous drag and allowing the central "jet" to preserve its forward momentum and extend further downstream before reattaching to the arterial wall.

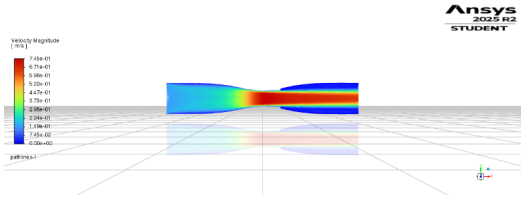


Figure 5: Non-Newtonian fluid streamlines

In contrast, the Newtonian model's -shown in Figure 6- constant viscosity assumption artificially increases resistance within the jet, causing premature flow reattachment. This difference is clinically critical, as the extended recirculation zone in the non-Newtonian model implies that a larger surface area of the vessel is exposed to low, oscillating shear stress—the primary hemodynamic environment known to promote endothelial dysfunction and accelerate secondary plaque deposition.

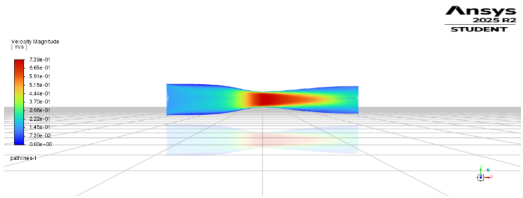


Figure 6: Newtonian fluid streamlines

## 6.1 Wall Shear Stress Analysis

A comparison of the peak WSS -shown in Figure 7- reveals that the Newtonian assumption slightly underestimates the stress (89.35 Pa) compared to the non-Newtonian model (89.43 Pa). Although the numerical difference is small ($\approx$ 0.1%), it reflects subtle shear-thinning effects at the stenotic throat. The convergence of peak WSS values between both models suggests that the very high shear rates in this region drive the non-Newtonian viscosity toward its infinite-shear limit ($\eta_\infty$), causing the flow to behave locally in a near-Newtonian manner. Consequently, a constant-viscosity model appears adequate at the throat itself but may fail to capture stress variations in adjacent lower-shear regions.

## 6.2 Bio-implication

These low-shear areas are clinically defined as "atheroprone"; the stagnant, swirling flow increases the residence time of lipids, facilitating their penetration into the endothelium. This mechanism promotes inflammation and further plaque accumulation, creating a vicious cycle where the existing stenosis actively fosters disease progression downstream.

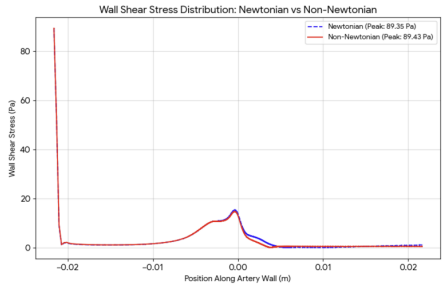


Figure 7: Wall Shear Stress distribution: Newtonian vs Non-Newtonian

# References

[1] Nichols, W. W., O'Rourke, M. F., & Vlachopoulos, C., *McDonald's Blood Flow in Arteries*, 6th ed., Hodder Arnold, 2011.

[2] Ku, D. N., "Blood flow in arteries," *Annual Review of Fluid Mechanics*, vol. 29, pp. 399–434, 1997.

[3] Schnyder, G. et al., "Common femoral artery anatomy," *Catheterization and Cardiovascular Interventions*, vol. 53, no. 3, pp. 289–295, 2001.

[4] Cho, Y. I., & Kensey, K. R., "Effects of the non-Newtonian viscosity of blood," *Biorheology*, vol. 28, pp. 241–262, 1991.